PERGAMON

International Journal of Solids and Structures 36 (1999) 763–783

INTERNATIONAL JOURNAL OF SOLIDS and STRUCTURES

Stresses around pin-loaded hole in composite laminates using direct boundary element method

Chien-Chang Lin*, Chuen-Horng Lin

Institute of Applied Mathematics, National Chung-Hsing University, Taichung, Taiwan, R.O.C.

Received 16 June 1997; in revised form 24 January 1998

Abstract

This study is concerned with stresses around a pin-loaded hole in symmetrically stacked composite laminates of finite size using a two-dimensional direct boundary element method. Effects of friction and clearance between the pin and hole edge on the stresses are accounted for. Also geometric compatibility and force constraint between the pin and the plate are enforced. A new relation for geometric compatibility is proposed. Stress distributions and the contact angle with slip and no-slip regions around the pin-loaded hole corresponding to various parameters are investigated. Some interesting results are obtained. The present method is effective and simple to use which can be implemented with a personal computer.

Keywords: Pin-loaded hole; Composite laminates; Stresses; Contact angle; Boundary element

Nomenclature

E_{11} Young's modules in the longitudinal direction
E_{22} Young's modules in the transverse direction
G_{12} shear modules
v_{12} Poisson's ratio
t surface traction
u displacement
D hole diameter
R hole radius
a pin radius
H thickness of the plate
W width of the plate
L length of the plate

* Corresponding author. Fax: 88642873028; e-mail: cclin@amath.nchu.edu.tw.

0020–7683/99/$ - see front matter
PII: S0020–7683(98)00045–6

d_1 edge distance between the hole center and the plate edge
A_{ij} stiffness constants
F_{ij} Green's function for traction
H_{ij} Green's function for displacement
μ coefficient of static friction
e clearance between the hole and the pin
δ pin displacement
ϕ polar angle with respect to the hole center
ψ polar angle with respect to the pin center
α one half of the total angle of contact
β one half of the contact angle of no-slip regions
u_x, u_y displacement components of the hole-edge
t_x, t_y traction components of the hole-edge
u_r radial displacement of the hole-edge
σ_r, $\tau_{r\phi}$ radial stresses of the hole-edge

1. Introduction

Increasing applications of composite materials in aircraft structures have motivated the investigation. The determination of the contact angle and stress distribution at the contact surface of pin-loaded composite laminate has been an important and challenging task for researchers. Limited work in this area is available in the open literature, and the authors are not aware of any existing closed form solutions for this problem concerning orthotropic plates. However, there are studies for stress and strength analyses for pin-loaded orthotropic plates using various numerical methods. Many authors assumed that the contact pressure at the boundary of the loaded hole varies as a cosine function and the pin is frictionless. Under these assumptions, Jong (1977), Zhang and Ueng (1984) used complex stress functions to obtain analytical solutions; Eshwar (1978), Ghosh and Rao (1981) considered clearance fit pin; Mangalgiri et al. (1987) analyzed the problem using an inverse technique. All of these analytical solutions considered the plate to be of infinite size. By finite element method for finite sized plates, Wong and Matthews (1981) studied bolted joints in a fiber reinforced plate, Chang et al. (1983, 1984a, b, 1986) studied the strength and failure mode of mechanically fastened fiber reinforced composite plates containing one- or two-loaded pins; Tsujimoto and Wilson (1986) made an elasto-plastic analysis of a pin-loaded composite laminate. Blackie and Chutima (1996) studied the stress distribution in pin connected composite laminate with multiple number of fasteners. Using a boundary element method, Mahajerin and Sikarskin (1986) analyzed the composite structures, principally for loaded hole in mechanically fastened composites. Lin and Lin (1993) investigated stress distribution in the plate and the strength of bolted joints of orthotropic plates under uniform inplane loading. Since, none of these studies addressed the pin-hole interaction as the pressure at the contact surface is pre-assumed to vary as a cosine function, their models are approximate.

There are studies accounting for the interaction between the pin and the hole. Hyer and Klang (1985), Hyer et al. (1987) gave an analytical solution to the problem of pin-loaded composite laminate in infinite size using a complex Fourier series in conjunction with boundary collocations

along the surface of contact between the pin and the hole edge. By finite element methods, Agarwal (1980) analyzed the stress distribution around the fastener hole and various modes of laminate failure; Rahman (1984) established regions of slip and no-slip along the surface of contact; an inverse formulation was used by Naik and Crews (1986) by maintaining displacement along the bolt-hole contact arc; Yogeswaren and Reddy (1988) determined the contact stresses and region for orthotropic plates by using a Lagrange multiplier method; Rahman and Rowlands (1993) considered a double-bolted mechanical joint of finite orthotropic laminate with the bolts in series in the direction of loading. Experimentally, Waszczak and Cruse (1971) investigated failure mode and strength of anisotropic bolt bearing specimens; Quinn and Matthews (1977) also measured the pin-bearing strength to investigate the effect of stacking sequence; Pyner and Matthews (1979) made comparisons of single and multi-hole bolted joint in glass fiber reinforced plastics; Tsai and Morton (1990) made a stress and failure analysis of a pin-loaded composite plate using contact stresses determined from experimentally measured displacements in conjunction with a finite element method; and Copper and Turvey (1995) investigated single bolt tension joints in pultruded GRP sheets.

The present study concerns with stress distribution and contact angle around a pin-loaded hole in composite laminates of finite size. Different from literature mentioned above, a direct boundary element method based on the fundamental solution given in Rizzo and Shippy (1970) and interacting equations of geometric compatibility as well as force constraint in contact region are used in the present analysis. Effects of applied load or pin displacement, hole size and clearance between the pin and hole edge on the contact angle consisting of slip and no-slip regions and the stresses in the contact region are investigated.

2. Stress analysis

2.1. *Statement of the contact problem*

The geometry and coordinate system for a finite pin-loaded plate considered in this study are shown in Fig. 1, where the origin of coordinate system is placed at the hole center O of plate before deformation. When a load P from the pin is gradually applied to the plate, the pin will first contact the hole-edge at one point ($\phi = 0$), then the contact will gradually spread over some region to a contact angle 2α causing the pin displacement δ due to plate deformation. In the present study, a clearance between the pin size of radius a and hole size of radius R and a rigid pin are considered. As a result, the center and radius of curvature of contact hole-edge after deformation will be different from those before deformation as shown in Fig. 1(b) and (c), where, for example, the points A_h, B_h on the hole edge and A_p, B_p, O_p on the pin will move to A'_h, B'_h, A'_p, B'_p, and O'_p after deformation with $A'_h = A'_p$ and $B'_h = B'_p$ being the points at the ends of slip contact region. Therefore, we propose the relation $R\phi = a\psi$ to identify the corresponding points of hole-edge before and after deformation with firm contact with the pin, where ϕ is the polar angle with respect to the hole center before deformation and ψ is the polar angle with respect to the pin center after deformation as shown in Fig. 1(b) and (c). This is different from the assumption $\psi = \phi$ used by Hyer and Klang (1985). The present assumption appears to be more reasonable, though the difference at final results would not be appreciable as the clearance and deformation are very small.

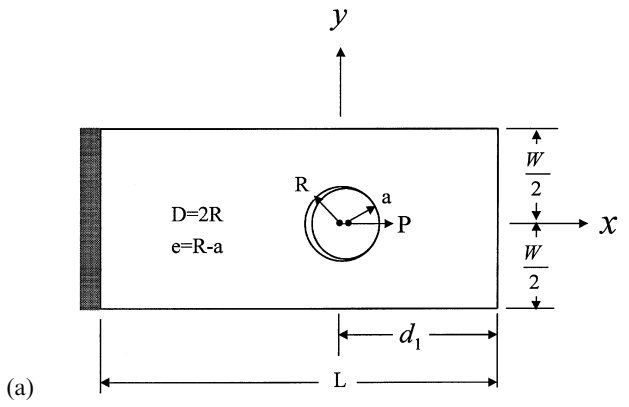

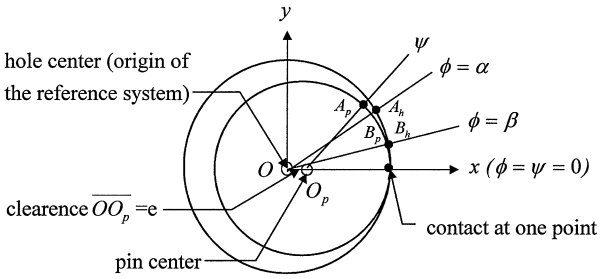

(b) Configuration of pin-loaded hole before deformation.

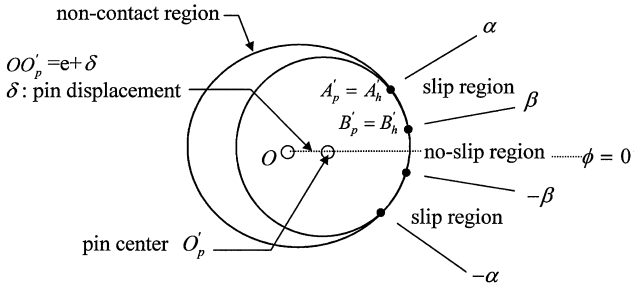

(c) Configuration of pin-loaded hole after deformation.

Fig. 1. Geometry and coordinate system for pin-loaded laminated.

The contact region is divided into two types of contact surfaces, slip region ($\beta \leqslant \phi < \alpha$ and $-\alpha < \phi \leqslant -\beta$) and no-slip region ($-\beta < \phi < \beta$), and the total angle 2α of contact region are described in Fig. 1(c). Compatibility in displacement must be satisfied on the no-slip contact surface ($-\beta < \phi < \beta$) by the relations

$$R\cos\phi + u_x = a\cos\left(\frac{R}{a}\phi\right) + (e+\delta) \quad (-\beta < \phi < \beta) \tag{1a}$$

$$R\sin\phi + u_y = a\sin\left(\frac{R}{a}\phi\right) \quad (-\beta < \phi < \beta) \tag{1b}$$

where u_x and u_y are displacements of the hole-edge in the x and y-directions, respectively; e is the clearance between the hole-edge and the pin before deformation. In the slip region ($\beta \leqslant \phi < \alpha$) and ($-\alpha < \phi \leqslant -\beta$), the geometric compatibility in radial direction of contact hole edge and force condition requiring that the friction force along the edge circumference is equal to the normal force multiplied by the friction coefficient between the pin and hole edge must be satisfied. The geometric compatibility is

$$\begin{aligned} u_r &= u_x\cos\phi + u_y\sin\phi \\ &= \left[e+\delta+a\cos\left(\frac{R}{a}\phi\right)\right]\cos\phi + a\sin\left(\frac{R}{a}\phi\right)\sin\phi \\ &\quad -R \quad (-\alpha < \phi \leqslant -\beta \text{ and } \beta \leqslant \phi < \alpha) \end{aligned} \tag{2a}$$

and the force condition is

$$|\tau_{r\phi}| = \mu|\sigma_r| \quad (-\alpha < \phi \leqslant -\beta \text{ and } \beta \leqslant \phi < \alpha) \tag{2b}$$

where u_r is the radial displacement of hole-edge, and μ is the coefficient of static friction between the pin and hole edge. And, of course, the stresses σ_r and $\tau_{r\phi}$ are zero along the non-contact hole-edge ($\alpha \leqslant \phi \leqslant 2\pi-\alpha$).

2.2. *Direct boundary element method* (*BEM*)

The direct BEM is formulated by the reciprocal work theorem. The theorem states that: if two distinct equilibrium states (ϕ_i^*, t_i^*, u_i^*) and (ϕ_i, t_i, u_i) exist in a region V bounded by the surface S, then the work done by the forces of the first state (*) on the displacements of the second state ( ) is equal to the work done by the forces of the second state on the displacements of the first state. Thus, according to Banerjee and Butterfield (1981), it can be represented by the following equation:

$$\int_S t_i^*(x)u_i(x)\,\mathrm{d}s(x) + \int_V \phi_i^*(z)u_i(z)\,\mathrm{d}V(z) = \int_S t_i(x)u_i^*(x)\,\mathrm{d}s(x) + \int_V \phi_i(z)u_i^*(z)\,\mathrm{d}V(z) \tag{3}$$

where x is a point on S, and z is a point in V. If u_i, t_i and ϕ_i are chosen as the actual state of displacements, traction, and body forces, respectively, then (*) is the state corresponding to a unit force $e^*(\xi)$ applied at ξ in an elastic body, and

$$\begin{aligned} t_i^*(x) &= F_{ij}(x,\xi)e_j^*(\xi) \\ u_i^*(x) &= H_{ij}(x,\xi)e_j^*(\xi) \end{aligned} \tag{4}$$

where F_{ij} and H_{ij} are Green's functions for traction and displacements, respectively, at a point x in the i direction due to a unit force applied at point ξ in the j direction. With the following manipulation by replacing $\phi_i^*(z)$ by $e_i^*(z)$ in the second term on the left hand side of eqn (3):

$$\int_V e_i^*(z)u_i(z)\,\mathrm{d}V(z) = \int_V e_i^*(\xi)\delta(z,\xi)u_i(z)\,\mathrm{d}V(z) = \int_V e_j^*(\xi)\delta_{ij}\delta(z,\xi)u_i(z)\,\mathrm{d}V(z) \tag{5}$$

where δ_{ij} is the Kronecker's delta, and $\delta(z,\xi)$ is the kernel function, eqn (3) becomes

$$\int_S F_{ij}(x,\xi)u_i(x)\,\mathrm{d}s(x) + \int_V \delta_{ij}\delta(z,\xi)u_i(z)\,\mathrm{d}V(z) = \int_S t_i(x)H_{ij}(x,\xi)\,\mathrm{d}s(x) + \int_V \phi_i(z)H_{ij}(z,\xi)\,\mathrm{d}V(z) \tag{6}$$

It should be noted that the common term $e_j^*(\xi)$ in each integral in eqn (6) has been dropped. Using the fact

$$\int_V \delta_{ij}\delta(z,\xi)u_i(z)\,\mathrm{d}V(z) = \int_V u_j(z)\delta(z,\xi)\,\mathrm{d}V(z) = \kappa u_j(\xi) \tag{7}$$

in which the value of κ equals one when point ξ is in V, 1/2 when ξ lies on S, and zero when ξ is outside of S. Thus, we can rewrite eqn (6) in the form

$$\kappa u_j(\xi) = \int_S [t_i(x)H_{ij}(x,\xi) - F_{ij}(x,\xi)u_i(x)]\,\mathrm{d}s(x) + \int_V \phi_i(z)H_{ij}(z,\xi)\,\mathrm{d}V(z) \tag{8}$$

Since no body force is considered in this study, hence

$$\kappa u_j(\xi) = \int_S [t_i(x)H_{ij}(x,\xi) - F_{ij}(x,\xi)u_i(x)]\,\mathrm{d}s(x) \tag{9}$$

which is the basis of integral formulations for the boundary element method used in the study.

2.3. *Fundamental solution*

A symmetrically stacked laminated plate consisting of N orthotropic laminae subjected to in-plane loads as shown in Fig. 1(a) is considered. The relationship between the in-plane stress resultants and the strain components based on the classical lamination theory is

$$\begin{Bmatrix} N_x \\ N_y \\ N_{xy} \end{Bmatrix} = \begin{bmatrix} A_{11} & A_{12} & A_{16} \\ A_{12} & A_{22} & A_{26} \\ A_{16} & A_{26} & A_{66} \end{bmatrix} \begin{Bmatrix} u_{x,x} \\ u_{y,y} \\ u_{x,y} + u_{y,x} \end{Bmatrix} \tag{10}$$

where

$$A_{ij} = \sum_{k=1}^{N} \bar{Q}_{ij}^{(k)} h_k$$

in which $\bar{Q}_{ij}^{(k)}$ are the reduced stiffnesses, and h_k is the thickness of the k-th layer.

If A_{16} and A_{26} are zero, eqn (10) reduces to

$$\begin{Bmatrix} N_x \\ N_y \\ N_{xy} \end{Bmatrix} = \begin{bmatrix} A_{11} & A_{12} & 0 \\ A_{12} & A_{22} & 0 \\ 0 & 0 & A_{66} \end{bmatrix} \begin{Bmatrix} u_{x,x} \\ u_{y,y} \\ u_{x,y}+u_{y,x} \end{Bmatrix} \tag{11}$$

which is the constitutive equation of the plane elasticity problem for a specifically orthotropic laminate.

The effective engineering properties for balanced and symmetric laminates are determined from the stiffness constants A_{ij}, such that the effective longitudinal Young's modules becomes $E_{11}=(A_{11}A_{22}-A_{12}^2)/A_{22}$, the transverse Young's modules $E_{22}=(A_{11}A_{22}-A_{12}^2)/A_{11}$, the longitudinal Poisson's ratio $v_{12}=A_{12}/A_{22}$, and the shear modules $G_{12}=A_{66}$.

The Hooke's law for plane stress state for orthotropic plates takes the form

$$u_{x,x}=S_{11}\sigma_x+S_{12}\sigma_y;\quad u_{y,y}=S_{12}\sigma_x+S_{22}\sigma_y;\quad u_{x,y}+u_{y,x}=S_{66}\sigma_{xy}$$

in which

$$S_{11}=\frac{1}{E_{11}};\quad S_{22}=\frac{1}{E_{22}};\quad S_{12}=\frac{-v_{12}}{E_{11}}=\frac{-v_{21}}{E_{22}};\quad S_{66}=\frac{1}{G_{12}} \tag{12}$$

The compliance S_{ij}, the stresses σ_{ij}, and the displacement gradients $u_{i,j}$ are taken as mean values through the thickness of the laminate.

According to Rizzo and Shippy (1970), various quantities F_{ij} and H_{ij} are taken as follows:

$$\begin{aligned}
H_{11} &= K_a(\sqrt{\rho_1}\bar{A}_2^2\ln\bar{r}_1-\sqrt{\rho_1}\bar{A}_1^2\ln\bar{r}_2)\\
H_{12} &= H_{21}=-K_a\bar{A}_1\bar{A}_2(\bar{\theta}_1-\bar{\theta}_2)\\
H_{22} &= -K_a\left(\frac{1}{\sqrt{\rho_1}}\bar{A}_1^2\ln\bar{r}_1-\frac{1}{\sqrt{\rho_2}}\bar{A}_2^2\ln\bar{r}_2\right)
\end{aligned} \tag{13}$$

$$\begin{aligned}
F_{11} &= K_a\left(\frac{\bar{A}_1}{\sqrt{\rho_2}r_2^2}-\frac{\bar{A}_2}{\sqrt{\rho_1}r_1^2}\right)(x_1n_1+x_2n_2)\\
F_{12} &= K_a\left(M_1\frac{\bar{A}_2}{\bar{r}_1^2}-M_2\frac{\bar{A}_1}{\bar{r}_2^2}\right)\\
F_{21} &= K_a\left(M_1\frac{\bar{A}_1}{\rho_1\bar{r}_1^2}-M_2\frac{\bar{A}_2}{\rho_2\bar{r}_2^2}\right)\\
F_{22} &= K_a\left(\frac{\bar{A}_1}{\sqrt{\rho_1}\bar{r}_1^2}-\frac{\bar{A}_2}{\sqrt{\rho_2}\bar{r}_2^2}\right)(x_1n_1+x_2n_2)
\end{aligned} \tag{14}$$

where

$$K_a = \frac{1}{2\pi(\rho_1-\rho_2)S_{22}}$$

$$\bar{A}_i = S_{12}-\rho_i S_{22}$$

$$\bar{r}_i = \sqrt{(x_1-\xi_1)^2+\frac{(x_2-\xi_2)^2}{\rho_i}}$$

$$\bar{\theta}_i = \tan^{-1}\left[\frac{(x_2-\xi_2)}{\sqrt{\rho_i}(x_1-\xi_1)}\right] \quad (i=1,2)$$

$$M_i = \sqrt{\rho_i}(x_1-\xi_1)n_2 - \frac{1}{\sqrt{\rho_i}}(x_2-\xi_2)n_1$$

and the values of ρ_i are determined from the following equations

$$\rho_1+\rho_2 = \frac{(2S_{12}+S_{66})}{S_{22}}$$

$$\rho_1\rho_2 = \frac{S_{11}}{S_{22}} \tag{15}$$

In the present study, the numerical values of ρ_i, for $i=1$ and 2, are assumed to be real and positive.

2.4. *Discretization of the boundary*

Upon dividing the boundary regions into M quadratic elements in eqn (9), each element has three nodes with two end nodes joined to adjacent elements. Each node of any element has two displacement components and two traction components. Considering the geometric compatibility, we used only two displacement components for each of end nodes joined to adjacent elements while four traction components are required to describe the force states at these end nodes. From eqn (9) we can relate the displacement vector of a nodal point p in terms of tractions or displacements at all ($2M$) nodal points on the boundary regions as

$$\frac{1}{2}\{u^p\} = \sum_{q=1}^{M}\left[\int_{S_q} H^{pq}N\,\mathrm{d}S\right]\{t^q\} - \sum_{q=1}^{M}\left[\int_{S_q} F^{pq}N\,\mathrm{d}S\right]\{u^q\} \quad (p=1,2,\ldots,2M) \tag{16}$$

where N is the shape function. Equation (16) can be represented by the simple matrix equation as follows:

$$[F]\{u\} = [H]\{t\} \tag{17}$$

in which $\{u^p\}$ has been merged into $\{u\}$, $[F]$ and $[H]$ are $4M\times 4M$ and $4M\times 6M$ matrices, respectively, $\{u\}$ and $\{t\}$ have the dimensions of $4M\times 1$ and $6M\times 1$, respectively. Using the $4M$ boundary conditions, which are either in tractions or displacements at all $2M$ nodes on the boundary elements, eqn (17) can be rewritten in the following form:

$$[A]\{X\} = [B]\{Y\} \tag{18}$$

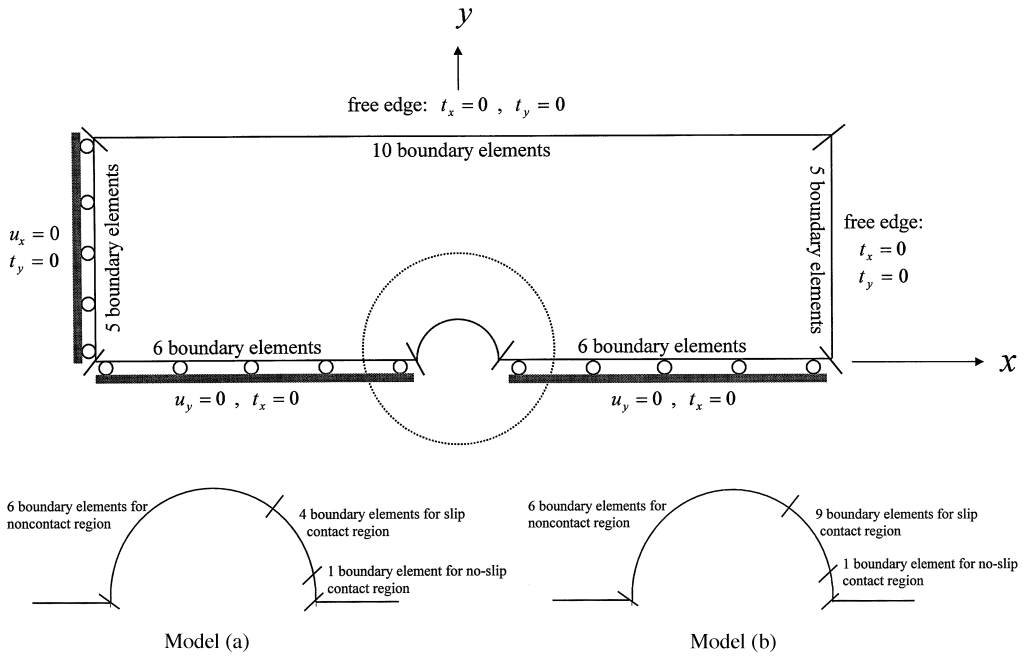

Fig. 2. Boundary element model for the pin-loaded laminates.

where $[A]$ is a $4M \times 4M$ matrix and $\{X\}$ contains the $4M$ unknown traction and displacement components, $[B]$ is a $4M \times 6M$ matrix, and $\{Y\}$ contains the given $6M$ boundary quantities.

2.5. *Boundary conditions and computation algorithm*

Because of the symmetry of the geometry, material properties, and loading, one half ($0 \leqslant y \leqslant W/2$) of plate is modeled with boundary elements as shown in Fig. 2. The given boundary conditions of the modeled half plate are as follows:

Along the edge $x = -L + d_1$ (for $0 \leqslant y \leqslant W/2$): $u_x = 0$ and $t_y = 0$ (19)

Along the boundary $y = 0$ (for $-L + d_1 \leqslant x \leqslant -R$ and $R \leqslant x \leqslant d_1$):

$$u_y = 0 \quad \text{and} \quad t_x = 0 \tag{20}$$

Along the edges $x = d_1$ (for $0 \leqslant y \leqslant W/2$); and $y = W/2$(for $-L + d_1 \leqslant x \leqslant d_1$):

$$t_x = 0 \quad \text{and} \quad t_y = 0 \tag{21}$$

Along the non-contact hole edge ($\alpha \leqslant \phi \leqslant 2\pi - \alpha$): $\sigma_r = \tau_{r\phi} = 0$ (22)

In addition, eqns (1a) and (1b) are used for the no-slip contact region around the hole, and eqns (2a) and (2b) are employed for the slip contact region. To accommodate the computation algorithm, we rewrite the eqn (2b) based on the relations:

$$\sigma_r = t_x \cos\phi + t_y \sin\phi, \quad \tau_{r\phi} = -t_x \sin\phi + t_y \cos\phi \tag{23}$$

in the following form:

$$t_y = \frac{(1+\mu^2)\sin\phi\cos\phi + \mu}{\cos^2\phi - \mu^2\sin^2\phi} t_x, \quad (-\alpha < \phi \leqslant -\beta \text{ and } \beta \leqslant \phi < \alpha) \tag{24}$$

The computation algorithm used for determining the contact angle and stresses along the contact surface of the hole edge is stated as follows:

Step 1. Input data including material properties, geometrical dimensions, friction coefficient μ, clearance e, and pin displacement δ.
Step 2. Assign values of angles α and β.
Step 3. Calculate the traction t_x, t_y and displacement u_x, u_y of nodal point on the boundary elements.
Step 4. Determine the angle ϕ of contact region for the nodal point along the hole edge.
Step 5. Calculate the stresses σ_r and $\tau_{r\phi}$ around the contact region of the hole according to eqns (23) and (24).
Step 6. Use the computed values of σ_r and $\tau_{r\phi}$ to check as to whether or not the force conditions of eqn (2b) for the angle β and of eqn (22) for the angle α are satisfied.
Step 7. Repeat steps 2–7 until a convergent solution is obtained.

3. Numerical results and discussions

To investigate the validity of the present method and effects of applied load or pin displacement, hole size and clearance on the contact angle and stresses around the contact region of the pin-loaded laminates, several examples are presented for illustrative purposes. For the sake of convenience in comparing with available results given in literature, the material properties of composites in all examples are chosen to be $E_{11} = 146.757$ GPa (21.3 Msi), $E_{22} = 10.8862$ GPa (1.58 Msi), $G_{12} = 6.4077$ GPa (20.93 Msi), $v_{12} = 0.38$. Three types of lamination 0°, $(0_2^\circ/\pm 45^\circ)_s$, and 90° as being selected by Hyer and Klang (1985) are considered. All of these laminates belong to the plane elasticity problems of a specially orthotropic laminate obeying the constitutive eqn (11). The geometrical dimensions of composite laminate are $L = W = 254$ mm, $d_1 = W/2 = 127$ mm, $H = 5.08$ mm; and the value of $\mu = 0.2$ for the coefficient of static friction between the pin and hole edge used by Hyer and Klang (1985) is selected for comparing the results. All stresses are non-dimensionalized with respect to the mean stress S as being used by Hyer and Klang (1985),

$$S = \frac{P}{DH} \tag{25}$$

where $D = 2R$, and H is the thickness of the plate.

To check the convergence and accuracy of the present boundary element model, two models of boundary element mesh as shown in Fig. 2 have been used. Model (a) has a total number of 43 boundary elements (with five elements meshed in the contact hole region), and model (b) has a total number of 48 boundary elements (with 10 elements meshed in the contact hole region).

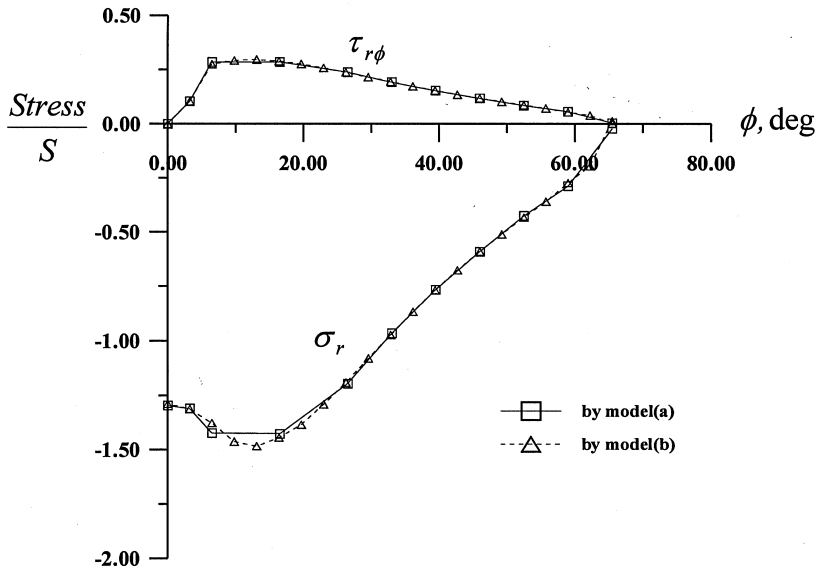

Fig. 3. Stresses around the pin-loaded hole in a 0° composite laminate with $\delta = 0.314$ mm ($S = 0.41$ GPa) and $e = 0.127$ mm.

Results using model (a) and model (b) for stresses around the pin-loaded hole in a 0° composite laminate are displayed in Fig. 3 which shows no significant discrepancies between these two results. For higher accuracy, results obtained by using model (b) are presented throughout all examples.

For comparison between the present results and the data given by Hyer and Klang (1985), stresses around the pin-loaded hole are determined for the 0°, $(0_2^\circ/\pm 45^\circ)_s$, and 90° composite laminates with pin radius $a = 12.573$ mm, hole radius $R = 12.7$ mm, pin displacement $\delta = 0.314$ mm, and $e = 0.127$ mm as used by Hyer and Klang (1985). These comparisons are shown in Figs 5–7. Present results show a similar trend to those in Hyer and Klang. The shearing stress $\tau_{r\phi}/S$ shows better agreements while some discrepancies appear for σ_r/S, and especially, significant differences appear for contact angles. The angles (2α) of contact region for these three laminates given by Hyer and Klang have the same value of about $\alpha = 74^\circ$, but are different in the present analysis at about 11.5, 16.2, and 23.0% less from 74° for 0°, $(0_2^\circ/\pm 45^\circ)_s$, and 90° laminates, respectively. The major contribution to the discrepancies may be due to the difference in the continuity condition used for the contact region for which $a\psi = R\phi$ is used in the present study while $\psi = \phi$ is considered in Hyer and Klang. In the present analysis using the relation $a\psi = R\phi$ ($R > a$), effects of clearance e and deformation along the contact hole-edge have been considered. It is shown by later examples that the effect of clearance reduces the contact angle and increases the stress σ_r along the center region of contact edge as the clearance e increases. Also, when a load is applied from the pin to laminate, the hole-edge will deform to fit the rigid pin with an arc length of the contact hole region equal to that on the rigid pin, so the angle ϕ with respect to the hole center is smaller than the corresponding angle ψ with respect to the pin center. The effect of deformation on the contact angle and stress distribution will be more significant for laminate with lower stiffness in the direction of loading as shown in Figs 4–6, where the most discrepancy between the present result

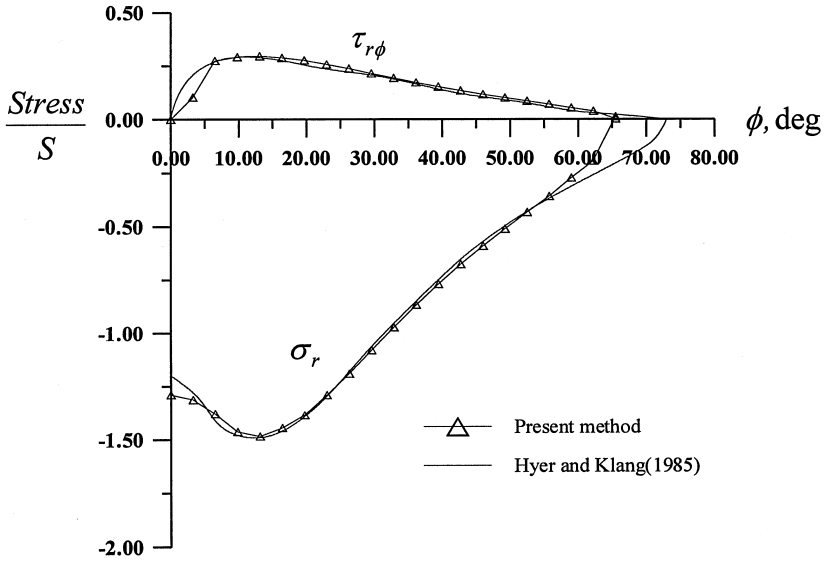

Fig. 4. Stresses around the pin-loaded hole in a 0° composite laminate with $\delta = 0.314$ mm ($S = 0.41$ GPa) and $e = 0.127$ mm.

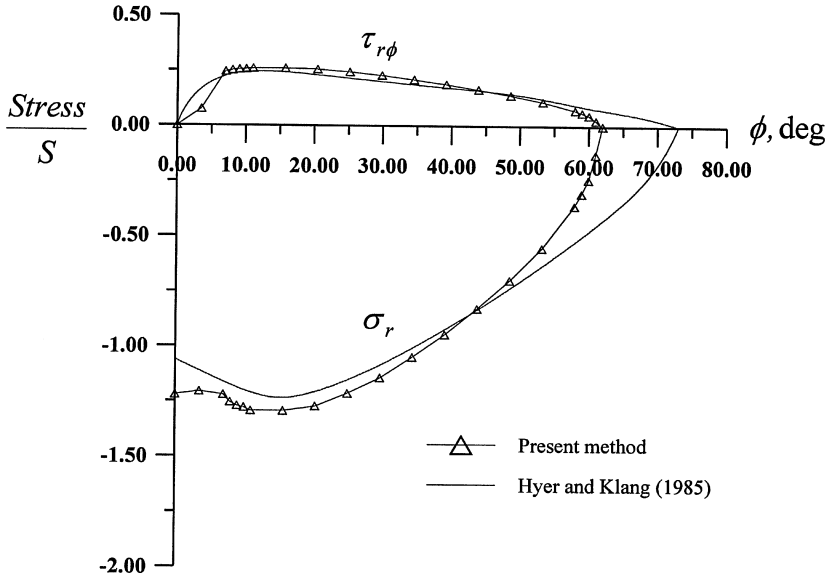

Fig. 5. Stresses around the pin-loaded hole in a $(0_2^\circ/\pm 45^\circ)_s$ composite laminate with $\delta = 0.314$ mm ($S = 0.43$ GPa) and $e = 0.127$ mm.

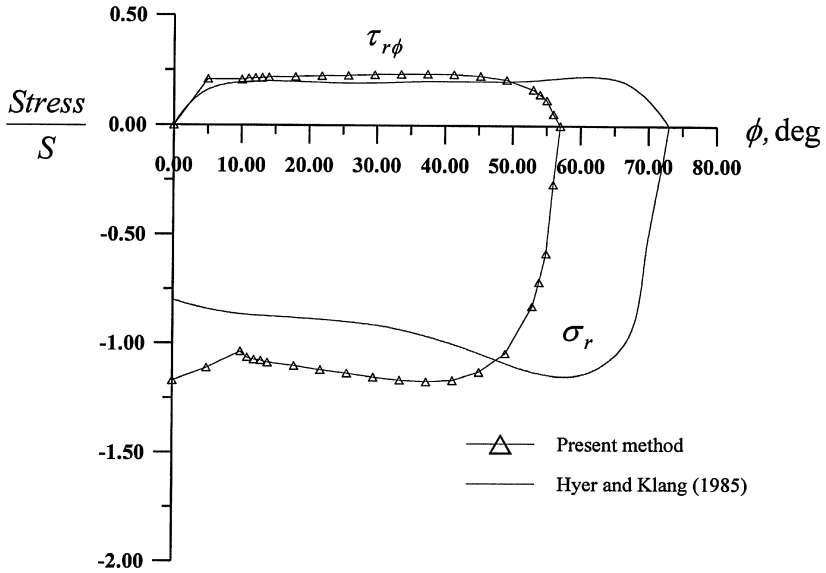

Fig. 6. Stresses around the pin-loaded hole in a 90° composite laminate with $\delta = 0.314$ mm ($S = 0.1$ GPa) and $e = 0.127$ mm.

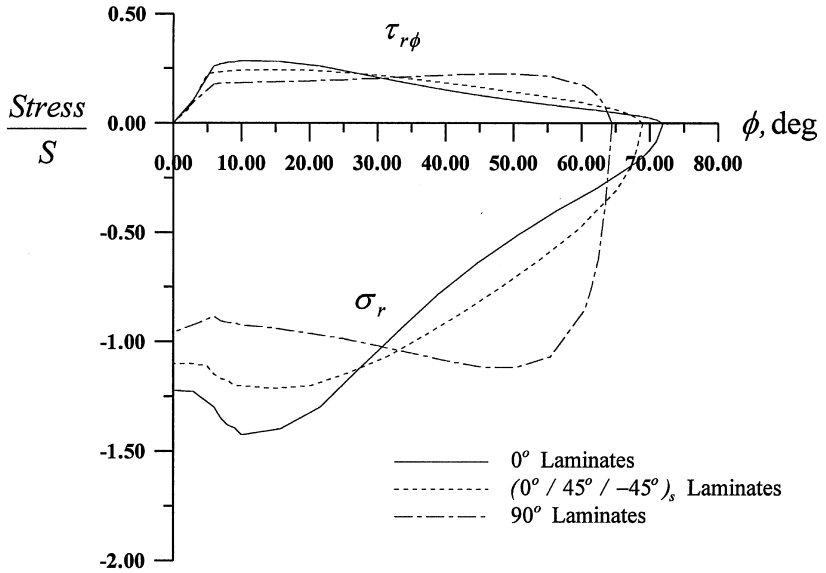

Fig. 7. Stresses around the pin-loaded hole in composite laminate of 0°, $(0_2^\circ/\pm 45^\circ)_s$, and 90° with $\delta = 0.5$ mm and $e = 0.127$ mm.

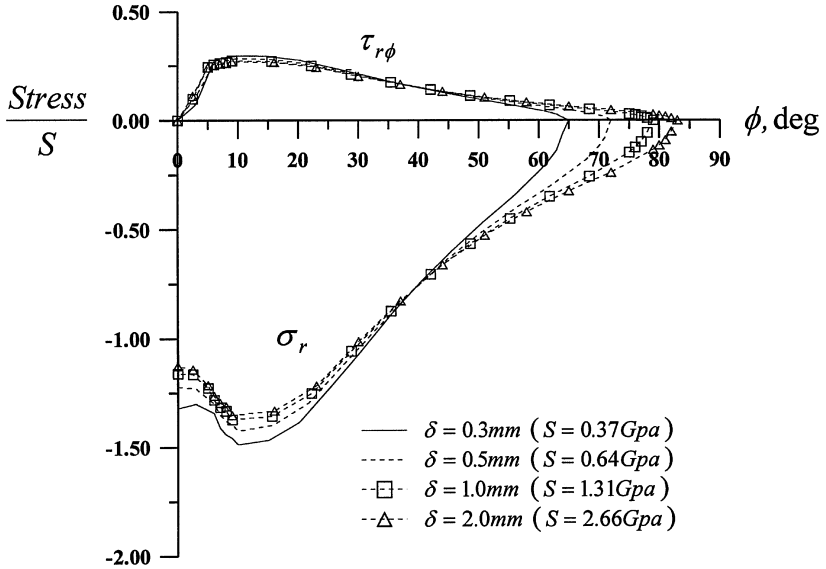

Fig. 8. Effect of pin-loaded displacement on stresses around the hole in a 0° composite laminate ($e = 0.127$ mm).

and Hyer and Klang (1985) appears for the 90° laminate. Present results reflect all the above facts, therefore, the present analysis using the relation $a\psi = R\phi$ is believed to be more reasonable. The analysis using the relation $\psi = \phi$ in the work by Hyer and Klang (1985) does not reflect the effects of clearance and hole edge deformation on the contact angle and stress distribution.

Next, we investigate the stress distributions around the pin-loaded hole under a load producing a deformation $\delta = 0.5$ mm for three different composite laminates having 0°, $(0_2^\circ/\pm 45^\circ)_s$, and 90° stacking sequences. The pin radius is $a = 12.573$ mm and the hole radius $R = 12.7$ mm. The stress distributions along the hole-edge are shown in Fig. 7. For σ_r/S, the trend for 0° and $(0_2^\circ/\pm 45^\circ)_s$ are similar for which the magnitude increases along the no-slip region from the center at $\phi = 0^\circ$ to the peak at about $\phi = 10^\circ$, and decreases along the slip region to zero at the end of contact surface. On the other hand, the magnitude of σ_r/S for 90° laminate first decreases slightly and gradually increases to its peak near the edge of the contact region as ϕ increases. Values of σ_r/S are about the same for all three laminates at about $\phi = 30^\circ$. For $\tau_{r\phi}/S$, the peak values occur near the center at about $\phi = 10^\circ$ for 0° and $(0_2^\circ/\pm 45^\circ)_s$ laminates, the variation for 90° laminate is nearly uniform. Again, curves cross near $\phi = 30^\circ$. While the 0° laminate exhibits the largest contact angle, the 90° laminate has the smallest. Values for β identifying the range of no-slip zones are 5°, 5.3° and 6° for 0°, $(0_2^\circ/\pm 45^\circ)_s$, and 90° laminates, respectively.

To investigate the influence of pin displacement δ due to hole deformation on the stresses, two different composite laminates of 0° and $(0_2^\circ/\pm 45^\circ)_s$ with various values of $\delta = 0.3$, 0.5, 1.0 and 2.0 mm are considered. The pin radius $a = 12.573$ mm, hole radius $R = 12.7$ mm are used. The effect of pin displacement δ on the stresses is shown in Figs 8 and 9. As expected the contact angle increases as the pin displacement increases. Variations of σ_r/S and $\tau_{r\phi}/S$ are essentially the same for all three laminates. The peak value of these nondimensionalized stresses occur near the center of the contact zones at about $\phi = 10^\circ$ which is the point in between the slip and no-slip region.

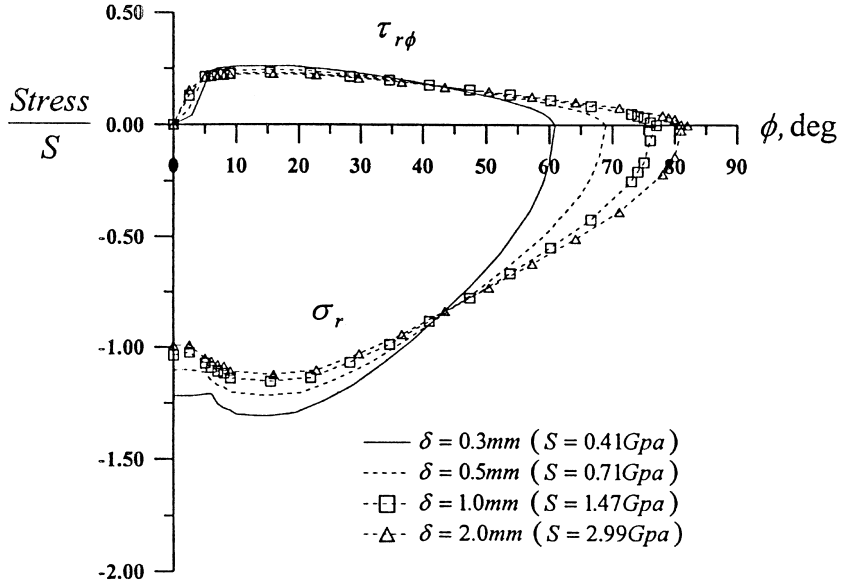

Fig. 9. Effect of pin-loaded displacement on stresses around the hole in a $(0_2^\circ/\pm 45^\circ)_s$ composite laminate with $e = 0.127$ mm.

The peak values increases as δ decreases. Curves corresponding to different values of δ cross at about $\phi = 40^\circ$.

Figures 10 and 11 illustrates the effect of pin/hole clearance on the hole-edge stresses. Two different composite laminates of 0° and $(0_2^\circ/\pm 45^\circ)_s$ with various pin/hole clearances of $e = 0.01$, 0.05 and 0.10 mm are considered. The hole radius is $R = 12.7$ mm, under a pin displacement $\delta = 0.314$ mm. Obviously, the contact angle decreases as the clearance increases. The radial stress σ_r/S increases as the clearance increases for the angle ϕ less than about 40° for 0° lamination, and 45° for $(0_2^\circ/\pm 45^\circ)_s$ lamination. The stress σ_r/S then decreases for larger values of ϕ. The stress $\tau_{r\phi}/S$ increases (along the no-slip region) from zero at $\phi = 0^\circ$ to the peak value at about $\phi = 10^\circ$ for all cases.

Figures 12 and 13 illustrates the effects of geometrical dimensions on the stress distribution. Two different composite laminates of 0° and $(0_2^\circ/\pm 45^\circ)_s$ with various hole sizes of $L/D = 5$, 10, 20, and 50 are investigated. The pin/hole clearance $e = 0.127$ mm and applied force produces a pin displacement $\delta = 0.314$ mm are considered. The stress σ_r/S increases as L/D increases before the angle $\phi = 17^\circ$ and $\phi = 33^\circ$ in the contact zone for 0° and $(0_2^\circ/\pm 45^\circ)_s$ lamination, respectively. The stress σ_r/S increases as L/D decreases for larger values of ϕ. The stresses $\tau_{r\phi}/S$ along the polar angle ϕ increases on no-slip region to the peak value at about $\phi = 6^\circ$.

Finally, we investigate the effects of pin displacement δ, pin/hole clearance e and hole size L/D on the contact angle. Results for two different composite laminates of 0° and $(0_2^\circ/\pm 45^\circ)_s$ with various pin displacements are shown in Fig. 14. The contact angle increases rapidly when the pin displacement increases from $\delta = 0.1$–0.5 mm and then gradually increases to a contact value $\alpha = 83.5^\circ$ for 0° lamination, and to 81.5° for $(0_2^\circ/\pm 45^\circ)_s$ lamination when pin displacement reaches to $\delta = 2.0$ mm. Figure 15 shows the effect of pin/hole clearance e. The contact angle decreases

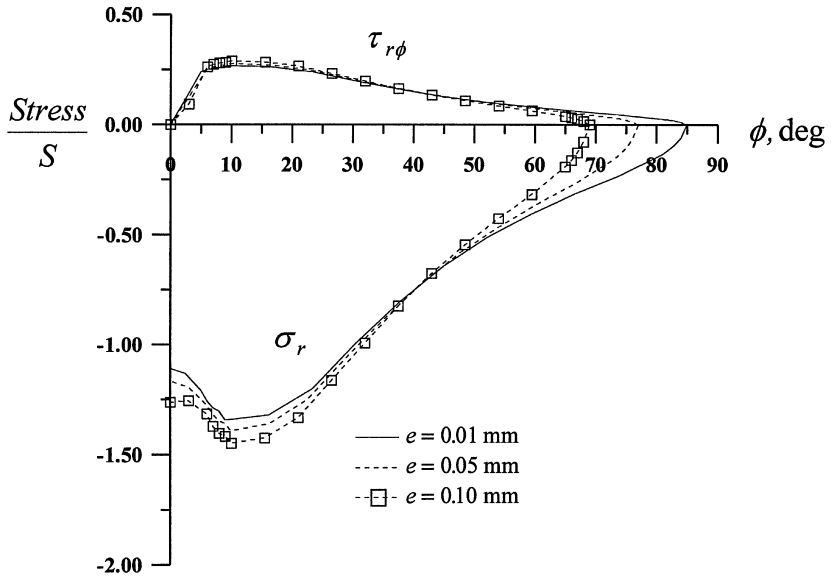

Fig. 10. Effect of pin-loaded clearance on stresses around the hole in a 0° composite laminate with $\delta = 0.314$ mm ($S = 0.41$ GPa).

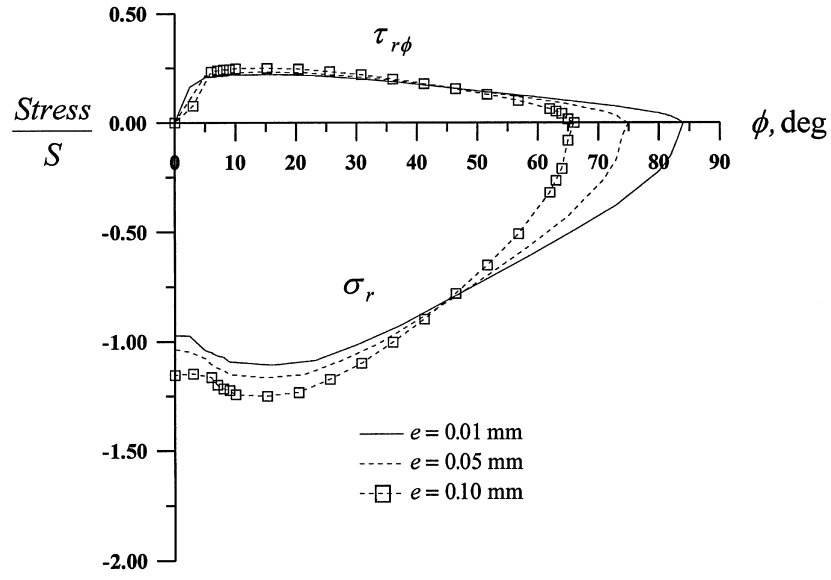

Fig. 11. Effect of pin-loaded clearance on stresses around the hole in a $(0_2^\circ/\pm 45^\circ)_s$ composite laminate with $\delta = 0.314$ mm ($S = 0.44$ GPa).

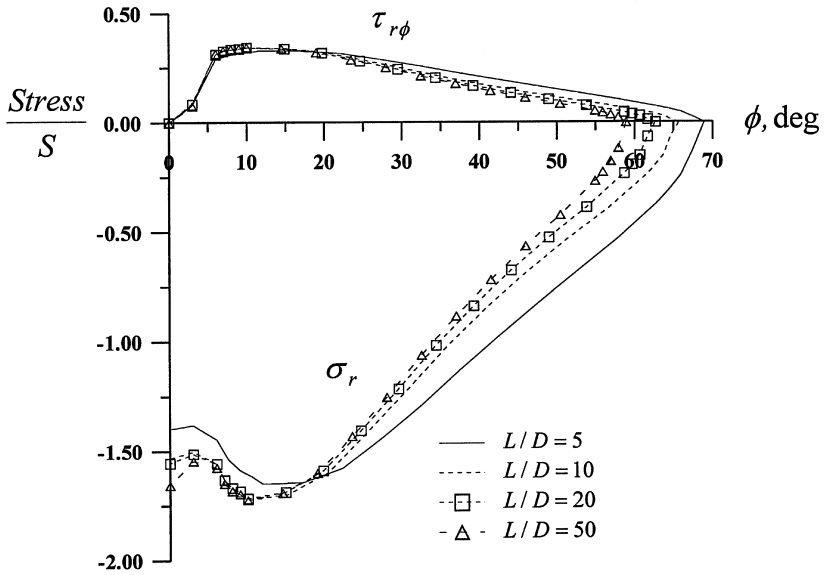

Fig. 12. Effect of hole size L/D on stresses around the hole in a 0° composite laminate with $\delta = 0.314$ mm and $e = 0.127$ mm.

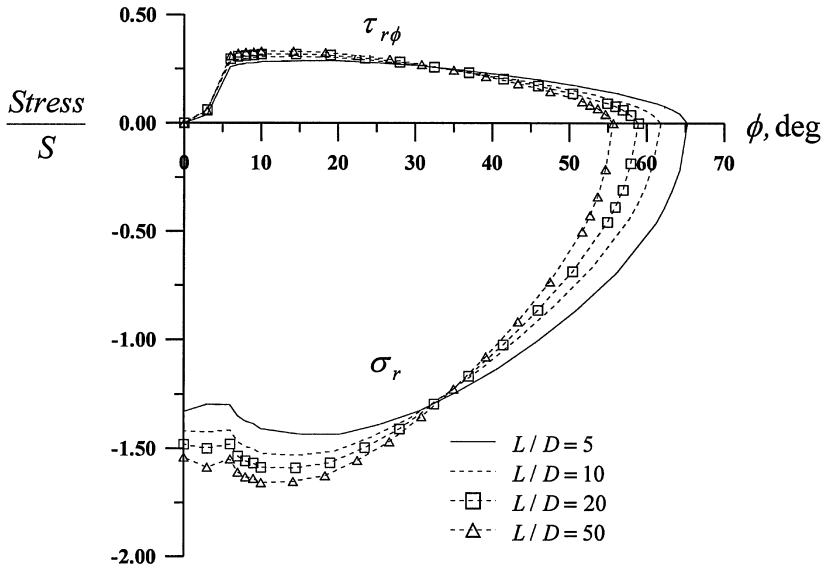

Fig. 13. Effect of hole size L/D on stresses around the hole in a $(0_2^\circ/\pm 45^\circ)_s$ composite laminate with $\delta = 0.314$ mm and $e = 0.127$ mm.

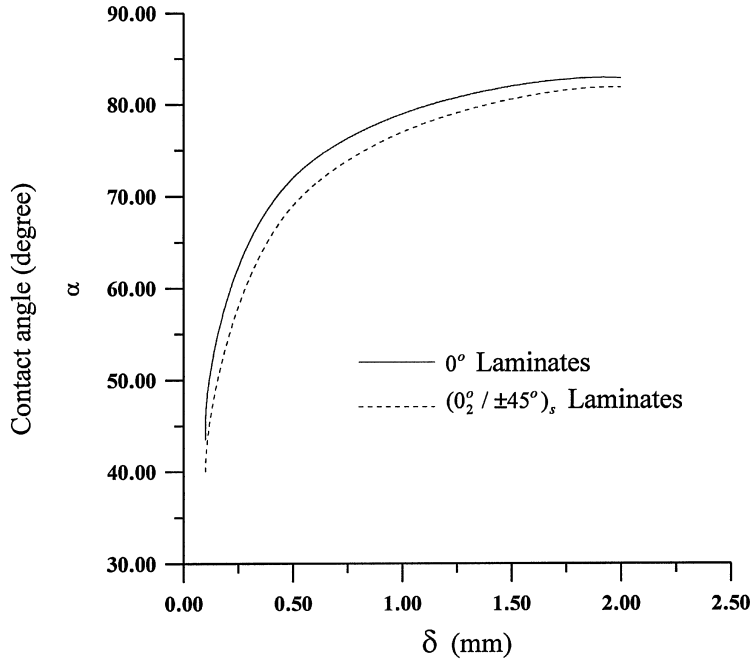

Fig. 14. Effect of pin-loaded displacement on contact angle with $e = 0.127$ mm.

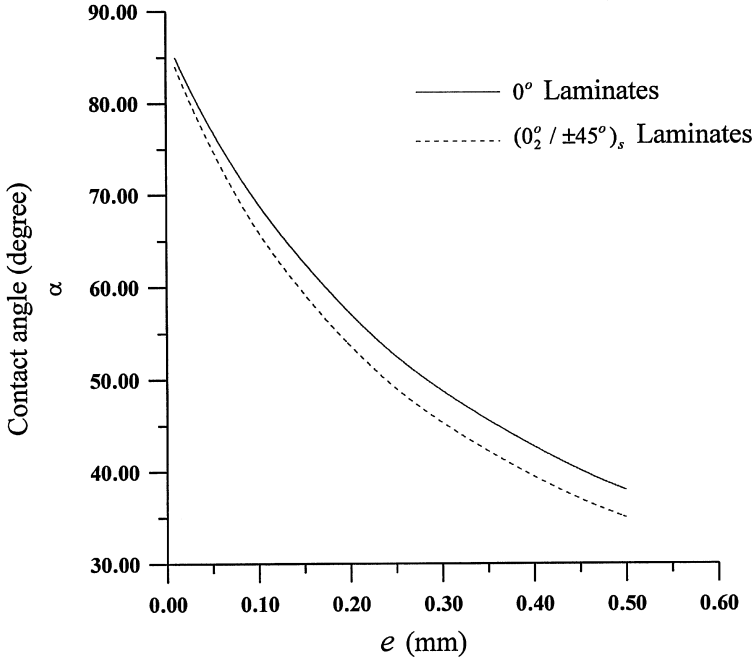

Fig. 15. Effect of pin-loaded clearance on contact angle with $\delta = 0.314$ mm.

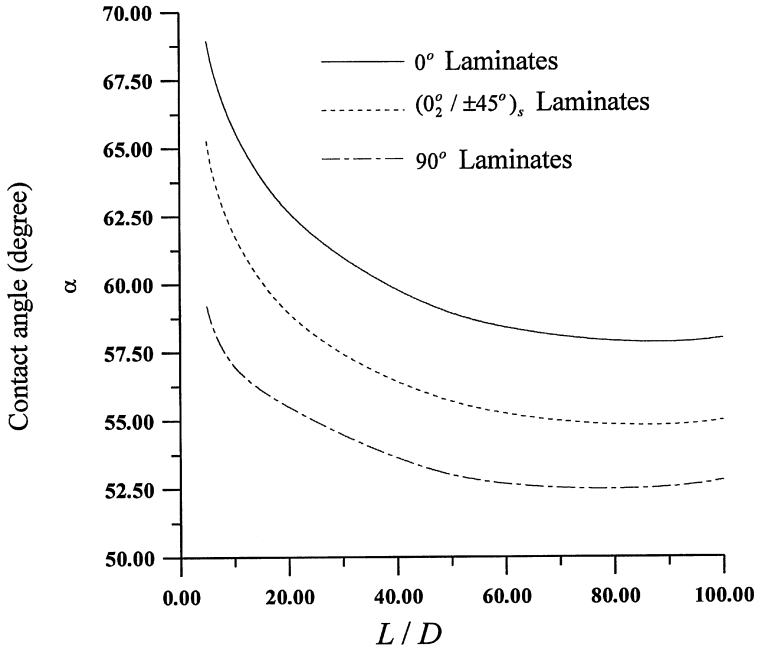

Fig. 16. Effect of hole size L/D on contact angle with $\delta = 0.314$ mm and $e = 0.127$ mm.

rapidly from $\alpha = 86^\circ$ to $\alpha = 38^\circ$ for 0° lamination, and to 36° for $(0_2^\circ/\pm 45^\circ)_s$ laminate as e increases from 0.1–0.5 mm. Figure 16 shows the effect of L/D. It shows that the contact angle is greater for larger pin/hole and reduces to a constant value as the pin/hole size is very small in comparison with the plate dimensions.

It is noted that many curves presented do not seem to be smooth enough. This is because only one element mesh is used for no-slip contact region, at about 0–10° for most examples in the boundary element model as shown in Fig. 2 used for the computations.

The computing time used on a personal computer (486DX2-66) for each case discussed above is recorded at about one minute.

4. Conclusions

An analysis method for determining the contact angle and stress distribution around the pin-loaded hole in finite composite laminates has been established by employing a two-dimensional direct boundary element method based on the proposed geometrical compatibility and force constraint conditions in contact region. In describing the geometrical compatibility, we have proposed the relation $a\psi = R\phi$ to identify the corresponding points of hole-edge before and after deformation for the firm contact between the pin and hole edge. This proposed relation, different from previous works given by other investigators, has reflected the effects of pin/hole clearance and loaded hole deformation on the contact angle and stress distribution. Various examples concerned with the effects of pin/hole clearance, pin load or displacement, hole size, and lamination

type on the contact angle and stress distribution have been investigated. From the results obtained for these examples, some conclusions can be made as follows:

(1) The present analysis using the relation $a\psi = R\phi$ reflects more realistically than $\psi = \phi$ assumption the effects of pin/hole clearance and loaded-hole deformation on the contact angle and stress distribution, and the results are reasonable.
(2) The effect of clearance reduces the contact angle and increases the stress near the center contact region as the clearance increases.
(3) The effect of the use of $a\psi = R\phi$ relation vs $\psi = \phi$ assumption on the contact angle and stress distribution is more significant for laminate with lower stiffness in the direction of loading. Values computed on the basis of present relation is smaller for contact angle and higher for stress in comparison with results computed using $\psi = \phi$ assumption for a given pin-loaded laminate.
(4) In the present analysis, results show that a larger pin displacement δ and/or smaller clearance e and/or greater pin/hole size L/D produces a larger contact region, and the contact angle and stress distribution depend on the type of laminates.
(5) The present study is limited to symmetrically stacked orthotropic laminates loaded by rigid pin, and plane stress state is considered.
(6) For more accurate stress distribution in the no-slip contact region, more elements meshed for this region are needed.
(7) The present method requiring minimal computational efforts is effective and efficient.

Acknowledgement

This study is supported by the National Science Council of the Republic of China under the Grant No. NSC83-0401-E005-029 and No. NSC84-2212-E005-012.

References

Agarwal, B.L., 1980. Static strength prediction of bolted joint in composite material. AIAA Journal 18 (11), 1371–1375.
Banerjee, P.K., Butterfield, R., 1981. Boundary Element Method in Engineering Science. McGraw-Hill, Berkshire, U.K.
Blackie, A.P., Chutima, S., 1996. Stress distributions in multi-fastened composite plates. Composite Structures 34, 427–436.
Chang, F.K., Scott, R.A., Springer, G.S., 1983. Strength of mechanically fastened composite joints. Journal of Composite Materials 16, 470–494.
Chang, F.K., Scott, R.A., 1984a. Failure of composite laminates containing pin loaded holes—method of solution. Journal of Composite Materials 18, 255–278.
Chang, F.K., Scott, R.A., 1984b. Failure strength of nonlinearly elastic composite laminates containing a pin loaded hole. Journal of Composite Materials 18, 464–477.
Chang, F.K., 1986. The effect of pin load distribution on the strength of pin loaded holes in laminated composites. Journal of Composite Materials 20, 401–408.
Cooper, C., Turvey, G.J., 1995. Effects of joint geometry and bolt torque on the structural performance of single bolt tension joints in pultruded GRP sheet material. Composite Structures 32, 217–226.
Eshwar, V.A., 1978. Analysis of clearance fit pin joints. International Journal of Mech. Sci. 20, 485–491.
Ghosh, B.D., Rao, A.K., 1981. Load transfer from a smooth elastic pin to a large sheet. AIAA Journal 18 (5), 619–625.

Hyer, M.W., Klang, E.C., 1985. Contact stresses in pin-loaded orthotropic plates. International Journal of Solids and Structure 21 (9), 957–975.

Hyer, M.W., Klang, D.C., Cooper, D.E., 1987. The effects of pin elasticity, clearance, and friction on the stresses in a pin-loaded orthotropic plate. Journal of Composite Materials 21, 190–206.

Jong, T.D., 1977. Stresses around pin-loaded holes in elastically orthotropic or isotropic plates. Journal of Composite Materials 11, 313–331.

Lin, C.C., Lin, C.H., 1993. Stress and strength analysis of bolted composite joints using direct boundary element method. Journal of Composite Structures 25, 209–215.

Mahajerin, E., Sikarskin, D.L., 1986. Boundary element study of a loaded hole in an orthotropic plate. Journal of Composite Materials 20, 375–389.

Mangalgiri, P.D., Ramamurthy, T.S., Dattaguru, B., Rao, A.K., 1987. Elastic analysis of pin joints in plates under some combined pin and plate loads. International Journal Mech. Sci. 29 (8), 577–585.

Naik, R.A., Crews, J.H. Jr., 1986. Stress analysis method for a clearance-fit bolt. AIAA Journal 24 (8), 1348–1353.

Pyner, G.R., Matthews, F.L., 1979. Comparison of single and multi-hole bolted joints in glass fibre reinforced plastic. Journal of Composite Materials 13, 232–239.

Quinn, W.J., Matthews, F.L., 1977. The effect of stacking sequence on the pin-bearing strength in glass fibre reinforced plastic. Journal of Composite Materials 11, 139–145.

Rahman, M.U., 1984. An iterative procedure for finite-element stress analysis of frictional contact problems. Computers and Structures 18, 947–954.

Rahman, M.U., Rowlands, R.E., 1993. Finite element analysis of multiple bolted joints in orthotropic plates. Computers and Structures 46 (5), 859–867.

Rizzo, F.J., Shippy, D.J., 1970. A method for stress determination in plane anisotropic elastic bodies. Journal of Composite Materials 4, 36–61.

Tsai, M.Y., Morton, J., 1990. Stress and failure analysis of pin-loaded composite plate : an experimental study. Journal of Composite Materials 24, 1101–1121.

Tsujimoto, Y., Wilson, D., 1986. Elasto-plastic failure analysis of composite bolted joints. Journal of Composite Materials 20, 236–252.

Waszczak, J.P., Cruse, T.A., 1971. Failure mode and strength predictions of anisotropic bolt bearing specimens. Journal of Composite Materials 5, 421–425.

Wong, S., Matthews, F.L., 1981. A finite element analysis of single and two-hole bolted joints in fibre reinforced elastic. Journal of Composite Materials 15, 481–491.

Yogeswaren, E.K., Reddy, J.N., 1988. A study of contact stresses in pin-loaded orthotropic plates. Computers and Structures 30 (5), 1067–1077.

Zhang, K.D., Ueng, C.E.S., 1984. Stresses around a pin-loaded hole in orthotropic plates. Journal of Composite Materials 18, 432–446.